Effective absorption enhancement in dielectric thin-films with embedded paired-strips gold nanoantennas

Zih-Ying Yang[1] and Kuo-Ping Chen[2,*]

[1] *Institute of Lighting and Energy Photonics, National Chiao Tung University, 301 Gaofa 3rd Road, Tainan 711, Taiwan*

[2] *Institute of Imaging and Biomedical Photonics, National Chiao Tung University, 301 Gaofa 3rd Road, Tainan 711, Taiwan*

[*] *kpchen@nctu.edu.tw*

Abstract: This study focuses on determining the optimized thickness of an absorbing thin-film with embedded gold nanoantennas, for absorption enhancement. Gold paired-strips nanoantennas with small gaps have been proposed for light trapping because of the high localized electric field in the gap due to resonance. Paired-strips nanoantennas with small gaps produce higher effective absorption compared to single-strip gratings. From the average absorption two-dimensional map, the absorption enhancement may increase by a factor of up to 20 for gold paired-strips nanoantennas embedded in a 100 nm thick P3HT:PCBM thin-film.

OCIS codes: (250.5403) Plasmonics; (160.3918) Metamaterials; (250.0250) Optoelectronics.

References and links

1. S. Dutta Choudhury, R. Badugu, K. Ray, and J. R. Lakowicz, "Steering fluorescence emission with metal-dielectric-metal Structures of Au, Ag, and Al," J. Phys. Chem. C **117**(30), 15798–15807 (2013).
2. P. K. Maharana, S. Bharadwaj, and R. Jha, "Electric field enhancement in surface plasmon resonance bimetallic configuration based on chalcogenide prism," J. Appl. Phys. **114**(1), 014304 (2013).
3. E. Filippo, D. Manno, A. Buccolieri, M. Di Giulio, and A. Serra, "Shape-dependent plasmon resonances of Ag nanostructures," Superlattices Microstruct. **47**(1), 66–71 (2010).
4. W. S. Hwang, P. L. Truong, and S. J. Sim, "Size-dependent plasmonic responses of single gold nanoparticles for analysis of biorecognition," Anal. Biochem. **421**(1), 213–218 (2012).
5. B. C. Galarreta, I. Rupar, A. Young, and F. Lagugné-Labarthet, "Mapping hot-spots in hexagonal arrays of metallic nanotriangles with azobenzene polymer thin films," J. Phys. Chem. C **115**(31), 15318–15323 (2011).
6. M. D. Grogan, S. Heck, L. Xiao, R. England, S. Maier, and T. A. Birks, "Control of nanoparticle aggregation in aerogel hosts," J. Non-Cryst. Solids **358**(2), 241–245 (2012).
7. N. N. Nedyalkov, S. E. Imamova, P. A. Atanasov, and M. Obara, "Near field localization mediated by a single gold nanoparticle embedded in transparent matrix: application for surface modification," Appl. Surf. Sci. **255**(10), 5125–5129 (2009).
8. R. B. Dunbar, T. Pfadler, and L. Schmidt-Mende, "Highly absorbing solar cells–a survey of plasmonic nanostructures," Opt. Express **20**(S2 Suppl 2), A177–A189 (2012).
9. W. Challener, C. Peng, A. Itagi, D. Karns, W. Peng, Y. Peng, X. Yang, X. Zhu, N. Gokemeijer, Y.-T. Hsia, G. Ju, R. E. Rottmayer, M. A. Seigler, and E. C. Gage, "Heat-assisted magnetic recording by a near-field transducer with efficient optical energy transfer," Nat. Photonics **3**(4), 220–224 (2009).
10. L. Pan and D. B. Bogy, "Data storage: Heat-assisted magnetic recording," Nat. Photonics **3**(4), 189–190 (2009).
11. P. K. Jain, X. Huang, I. H. El-Sayed, and M. A. El-Sayed, "Noble metals on the nanoscale: optical and photothermal properties and some applications in imaging, sensing, biology, and medicine," Acc. Chem. Res. **41**(12), 1578–1586 (2008).
12. K. A. Willets and R. P. Van Duyne, "Localized surface plasmon resonance spectroscopy and sensing," Annu. Rev. Phys. Chem. **58**(1), 267–297 (2007).
13. L.-Y. Yue, P. Wang, and Y.-X. Huang, "Easy method to determine refractive indices of microspheres and in micro-regions of inhomogeneous media," Biosens. Bioelectron. **30**(1), 216–222 (2011).
14. M. A. Green and S. Pillai, "Harnessing plasmonics for solar cells," Nat. Photonics **6**(3), 130–132 (2012).
15. N. A. Hatab, C.-H. Hsueh, A. L. Gaddis, S. T. Retterer, J.-H. Li, G. Eres, Z. Zhang, and B. Gu, "Free-standing optical gold bowtie nanoantenna with variable gap size for enhanced Raman spectroscopy," Nano Lett. **10**(12), 4952–4955 (2010).

#205580 - $15.00 USD Received 10 Feb 2014; revised 28 Apr 2014; accepted 8 May 2014; published 19 May 2014

16. M. Li, S. K. Cushing, J. Zhang, J. Lankford, Z. P. Aguilar, D. Ma, and N. Wu, "Shape-dependent surface-enhanced Raman scattering in gold-Raman probe-silica sandwiched nanoparticles for biocompatible applications," Nanotechnology **23**(11), 115501 (2012).
17. J. M. McMahon, S. Li, L. K. Ausman, and G. C. Schatz, "Modeling the effect of small gaps in surface-enhanced Raman spectroscopy," J. Phys. Chem. C **116**(2), 1627–1637 (2012).
18. D. K. Gramotnev, A. Pors, M. Willatzen, and S. I. Bozhevolnyi, "Gap-plasmon nanoantennas and bowtie resonators," Phys. Rev. B **85**(4), 045434 (2012).
19. V. E. Ferry, M. A. Verschuuren, H. B. Li, E. Verhagen, R. J. Walters, R. E. Schropp, H. A. Atwater, and A. Polman, "Plasmonic light trapping for thin film A-SI: H solar cells," in *Proceedings of Photovoltaic Specialists Conference (PVSC),* (IEEE, 2010), pp. 000760–000765.
20. C. Mu, J.-P. Zhang, and D. Xu, "Au nanoparticle arrays with tunable particle gaps by template-assisted electroless deposition for high performance surface-enhanced Raman scattering," Nanotechnology **21**(1), 015604 (2010).
21. K. Q. Costa and V. Dmitriev, "Comparative analysis of circular and triangular gold nanodisks for field enhancement applications," J. Micro. Optoelectron. Electromagn. Appl. **9**(2), 123–130 (2010).
22. T. L. dos Santos, K. Q. da Costa, and V. Dmitriev, "Comparative Near Field Analysis of Gold Nanodisks of Different Shapes," in *Latin America Optics and Photonics Conference*(Optical Society of America, 2010).
23. H.-W. Cheng and Y. Li, "Simulation of Raman enhancement in SERS-active substrates with Au layer considering different geometry of nanoparticles," in *Proceedings of Computational Electronics (IWCE),* (IEEE, 2010), pp. 1–4.
24. G. Bi, W. Xiong, L. Wang, K. Ueno, H. Misawa, and J.- Qiu, "Fabrication of periodical structure and shape-induced modulating spectroscopy of Au nanoparticles," Opt. Commun. **285**(9), 2472–2477 (2012).
25. R.-H. Fan, L.-H. Zhu, R.-W. Peng, X.-R. Huang, D.-X. Qi, X.-P. Ren, Q. Hu, and M. Wang, "Broadband antireflection and light-trapping enhancement of plasmonic solar cells," Phys. Rev. B **87**(19), 195444 (2013).
26. V. E. Ferry, J. N. Munday, and H. A. Atwater, "Design considerations for plasmonic photovoltaics," Adv. Mater. **22**(43), 4794–4808 (2010).
27. R. A. Pala, J. White, E. Barnard, J. Liu, and M. L. Brongersma, "Design of Plasmonic Thin-Film Solar Cells with Broadband Absorption Enhancements," Adv. Mater. **21**(34), 3504–3509 (2009).
28. W. Wang, S. Wu, K. Reinhardt, Y. Lu, and S. Chen, "Broadband light absorption enhancement in thin-film silicon solar cells," Nano Lett. **10**(6), 2012–2018 (2010).
29. P. B. Johnson and R.-W. Christy, "Optical constants of the noble metals," Phys. Rev. B **6**(12), 4370–4379 (1972).
30. X. Ni, Z. Liu, and A. V. Kildishev, "PhotonicsDB: Optical Constants," (2010), *https://nanohub.org/resources/PhotonicsDB*.
31. S.-J. Tsai, M. Ballarotto, D. B. Romero, W. N. Herman, H.-C. Kan, and R. J. Phaneuf, "Effect of gold nanopillar arrays on the absorption spectrum of a bulk heterojunction organic solar cell," Opt. Express **18**(S4 Suppl 4), A528–A535 (2010).
32. H. A. Atwater and A. Polman, "Plasmonics for improved photovoltaic devices," Nat. Mater. **9**(3), 205–213 (2010).
33. F. Cortés-Juan, C. C. Ramos, J. Connolly, C. David, F. G. de Abajo, J. Hurtado, V. Mihailetchi, S. Ponce-Alcántara, and G. Sánchez, "Effect of Ag nanoparticles integrated within antireflection coatings for solar cells," J. Renewable Sustainable Energy **5**(3), 033116 (2013).
34. V. Gusak, B. Kasemo, and C. Hägglund, "Thickness dependence of plasmonic charge carrier generation in ultrathin a-Si:H layers for solar cells," ACS Nano **5**(8), 6218–6225 (2011).
35. B. Johansen, C. Uhrenfeldt, and A. N. Larsen, "Plasmonic properties of β-Sn Nanoparticles in ordered and disordered arrangements," Plasmonics **8**, 1–6 (2013).
36. J. Toudert, R. Serna, and M. Jiménez de Castro, "Exploring the optical potential of nano-bismuth: tunable surface plasmon resonances in the near ultraviolet-to-near infrared range," J. Phys. Chem. C **116**(38), 20530–20539 (2012).
37. O. A. Yeshchenko, I. M. Dmitruk, A. A. Alexeenko, A. V. Kotko, J. Verdal, and A. O. Pinchuk, "Size and temperature effects on the surface plasmon resonance in silver nanoparticles," Plasmonics **7**(4), 685–694 (2012).
38. C. Perera and K. Vernon, "Simulation of the gap plasmon coupling with a quantum dot," Proc. SPIE **8923**, 89230Z (2013).
39. K. Q. Le, A. Abass, B. Maes, P. Bienstman, and A. Alù, "Comparing plasmonic and dielectric gratings for absorption enhancement in thin-film organic solar cells," Opt. Express **20**(S1), A39–A50 (2012).
40. D. Qu, F. Liu, Y. Huang, W. Xie, and Q. Xu, "Mechanism of optical absorption enhancement in thin film organic solar cells with plasmonic metal nanoparticles," Opt. Express **19**(24), 24795–24803 (2011).
41. W. Ren, G. Zhang, Y. Wu, H. Ding, Q. Shen, K. Zhang, J. Li, N. Pan, and X. Wang, "Broadband absorption enhancement achieved by optical layer mediated plasmonic solar cell," Opt. Express **19**(27), 26536–26550 (2011).
42. F. Monestier, J.-J. Simon, P. Torchio, L. Escoubas, F. Flory, S. Bailly, R. de Bettignies, S. Guillerez, and C. Defranoux, "Modeling the short-circuit current density of polymer solar cells based on P3HT: PCBM blend," Sol. Energy Mater. Sol. Cells **91**(5), 405–410 (2007).
43. N. N. Lal, B. F. Soares, J. K. Sinha, F. Huang, S. Mahajan, P. N. Bartlett, N. C. Greenham, and J. J. Baumberg, "Enhancing solar cells with localized plasmons in nanovoids," Opt. Express **19**(12), 11256–11263 (2011).

#205580 - $15.00 USD Received 10 Feb 2014; revised 28 Apr 2014; accepted 8 May 2014; published 19 May 2014

44. M. Wang, C. Hu, M. Pu, C. Huang, Z. Zhao, Q. Feng, and X. Luo, "Truncated spherical voids for nearly omnidirectional optical absorption," Opt. Express **19**(21), 20642–20649 (2011).
45. Z. Chen, L. Wang, C. Wang, and Y. Zhu, "Polarization-insensitive surface plasmon resonance sensor by cross-slit metallic periodic arrays," Optik (Stuttg.) **124**(24), 6743–6745 (2013).
46. K. Aydin, V. E. Ferry, R. M. Briggs, and H. A. Atwater, "Broadband polarization-independent resonant light absorption using ultrathin plasmonic super absorbers," Nat Commun **2**, 517 (2011).
47. S. Y. Chou and W. Ding, "Ultrathin, high-efficiency, broad-band, omni-acceptance, organic solar cells enhanced by plasmonic cavity with subwavelength hole array," Opt. Express **21**(S1), A60–A76 (2013).
48. Y. Nishijima, L. Rosa, and S. Juodkazis, "Surface plasmon resonances in periodic and random patterns of gold nano-disks for broadband light harvesting," Opt. Express **20**(10), 11466–11477 (2012).

1. Introduction

At resonant frequencies, the oscillations of electrons at a metallic nanostructure's surface may produce an electric field enhancement, and the striking optical properties are called surface plasmon resonances (SPR). The characteristics of the resonances due to surface plasmons may be controlled by using different metals [1, 2], tuning the shape of the metal [3, 4], changing the polarization of the incident wave [5], and engineering the dielectric host [6, 7]. Surface plasmons provide two possible ways to enhance absorption when the metallic nanostructures are embedded in absorber layers. One is non-propagating electron excitations around the metallic nanostructures, called localized surface plasmons (LSPs), while another is bound electromagnetic waves propagating along the interfaces, called surface plasmon polaritons (SPPs) [8]. SPR has received much attention in recent years because of the localized high electric field intensity and the controllable resonance wavelength, which could be applied in ultra-high density data storage [9, 10], bio-sensing [11–13], efficient light-trapping [14], and surface-enhanced Raman scattering (SERS) [15–17].

A nanoantenna is one of the most attractive plasmonic nanostructures that could be used to not only receive and transmit but also confine and enhance the electromagnetic wave. As two nanoparticles are close to each other, additional enhancement occurs due to the small gap, which has attracted considerable attention [18–20]. Some geometries have been analyzed, such as circular disks, triangular disks [21], concave and convex triangles, curved side triangles with some tips [22], spherical, cubic, and pyramidical nanoparticles [23]. To understand the electromagnetic behavior, the individual nanoparticles' resonant responses, near-field and far-field distribution, and spectral responses have been investigated [8, 24]. Furthermore, some attention has been paid to analyze the electric field by integration, such as calculating the effective absorption (A_{slab}) in silicon thin-film solar cells using Eq. (1) [25–27],

$$A_{slab} = \frac{1}{2}\omega * \mathrm{Im}(\varepsilon)\oint_{v} |E|^2 \, dv' \tag{1}$$

where Im(ε) is the imaginary part of dielectric function of the absorber layer, $|E|$ is the magnitude of the electric field within the absorber layer, and v is the volume of the absorber layer.

By using Eq. (1), the effective absorption of a thin-film embedded with metal nanostructures could be calculated. However, there is less discussion on optimizing the thin-film thickness to achieve the maximum effective absorption [28]. Especially when surface plasmon resonance occurs, a strong localized electric field will be generated. Therefore, the thickness of the host will be an important factor to engineer and study. In this paper, gold paired-strips nanoantennas, with small gaps, and single-strip gratings are analyzed by simulation with a finite element method (FEM). Compared to other shapes of nanoantennas, paired-strips nanoantennas may be easily modeled in a two-dimensional (2D) environment, which is very convenient for studying effective absorption for different thicknesses of the host. Comparing the paired-strips nanoantennas to single-strip gratings, the localized electric field in the small gap of nanoantennas shows a strong effect on the absorption in the host. By

#205580 - $15.00 USD Received 10 Feb 2014; revised 28 Apr 2014; accepted 8 May 2014; published 19 May 2014

introducing the absorption formula, as in Eq. (1), the absorption is calculated as an index for optimized design. The dependence of absorption on the absorber layer's thickness and refractive index are discussed in detail.

2. Simulation method

This paper presents the plasmonic enhancement of gold paired-strips nanoantennas, and analyzes the enhancement factor with varying thickness of the surrounding medium. Paired-strips nanoantennas have the advantage of larger enhancement areas compared to bowtie nanoantennas. In addition, paired-strips nanoantennas are easier to fabricate, as sharp corners are not necessary. The solutions from the commercially available FEM package COMSOL (version 4.3) are used to investigate the electric field enhancement behavior by integral analysis. In the simulations, the calculations were set up as a 2D system with a built-in adaptive mesh. The mesh size of the spatial discretization is restricted to a maximum triangular side length of 5 nm and the element growth rate is 1.1, in both the metal and the absorber layer. In our simulation, the mesh is modified until the result no longer changes. Both single strip gold gratings and paired-strips gold nanoantennas are compared to a no metal structure model, acting as a reference. The optical constants of gold material are determined applying the data of Johnson and Christy from nanoHUB [29, 30]. As well as comparing the resonant properties and electric field distribution by averaging the integral electric field for distinct regions, the absorption (A_{slab}) in the absorber layer is calculated with Eq. (1). Furthermore, the absorption enhancement factor is used to investigate the optimized absorption by engineering the absorber layer.

Wang *et al.* used the normalized and time-averaged electric field to compare the absorption enhancement by varying a Si layer's thickness [28]. In order to further study the absorption enhancement for different host thicknesses, the result was divided by the absorber area to obtain the absorption per unit area. In this study, the average electric field of gold nanostructures sitting on the glass substrate in the air is calculated by Eq. (2).

$$E_{avg} = \frac{|E|}{\text{total area of integral region}} \tag{2}$$

where $|E|$ is the magnitude of the electric field using different heights of the integral region.

The average absorption per unit area ($A(\lambda)_{avg}$) of the dielectric absorber layer at any given wavelength is evaluated by Eq. (3).

$$A(\lambda)_{avg} = \frac{A_{slab}(\lambda)}{\text{total area}} \tag{3}$$

As well as comparing the average absorption per unit area ($A(\lambda)_{avg}$) for both paired-strips and single-strip nanostructures, the optimized absorption is considered by varying the thickness of the absorber layer.

3. Simulation results

3.1 Gold nanoantennas sitting on a glass substrate

The optical resonant properties in the vicinity of gold-pair-grating nanostructures are analyzed by a 2D FEM algorithm, which is a numerical solution based on Maxwell's equations and may be applied to obtain information about the electromagnetic field distribution in the near-field and far-field. Figures 1(a) and 1(b) are the geometries chosen for the configuration: the period is 400 nm, the width and thickness of each strip is 90 nm, the gap between paired-strips is 16 nm, and the paired-strips nanoantennas are sitting on a glass substrate (with refractive index n = 1.5). The gold nanoantennas are fabricated by e-beam lithography and a scanning electron microscope image of the sample is shown in Fig. 1(c).

#205580 - $15.00 USD Received 10 Feb 2014; revised 28 Apr 2014; accepted 8 May 2014; published 19 May 2014

The irradiation is a TM-wave (the electric field is across the gap), from the top with normal incidence. In Figs. 1(a) and 1(b), h represents the height of electric field's integral region. Normalized average electric field 2D maps for paired-strips nanoantenna and single-strip gratings are shown in Figs. 2(a) and 2(b). Comparing the different integrated thicknesses in surrounding medium, for the thicker slab (h = 1200 nm), there is only a slight enhancement at the resonant wavelength for structures shown in Figs. 1(a) and 1(b). The reason is clear because the concentrated electric field is only near the metal. For the thinner slab (h < 600 nm), the corresponding distribution of normalized average electric fields are shown in Figs. 2(c) and 2(d). Comparing structures shown in Figs. 1(a) and 1(b), in paired-strips gratings, the first enhancement peak occurs at the contact surface of the metal and substrate, with a slab thickness h = 20 nm and the normalized average electric field is 2.47. The second peak is at a slab thickness, h = 100 nm, and the normalized average electric field is 2.42. On the other hand, single-strip gratings only have the localized field at the contact surface, so there is only one peak at h = 20 nm, and the normalized average electric field is 1.73, which is 30% less than paired-strips nanoantennas. Based on the simulation results, paired-strips nanoantennas gratings can provide better resonance enhancement than single-strip gratings in thin-film absorber layers. It is also shown that the average electric field would be larger in the region near the substrate or on top of the nanoparticles, which can be used to engineer the effective slab thickness. On the other hand, the maximum electric fields around the metal in the air are also calculated. Figure 3 shows the maximum electric field spectra for single-strip and paired-strips structures, using both TE and TM illumination. It is evident from the results that the paired-strips nanoantennas have the stronger average electric field, which is 51% higher than for the single-strip. Clearly, the resonance would happen only under TM illumination. In addition, the maximum electric field would occur around a wavelength of 600 nm for both single-strip gratings and paired-strips nanoantennas, when using a TM wave.

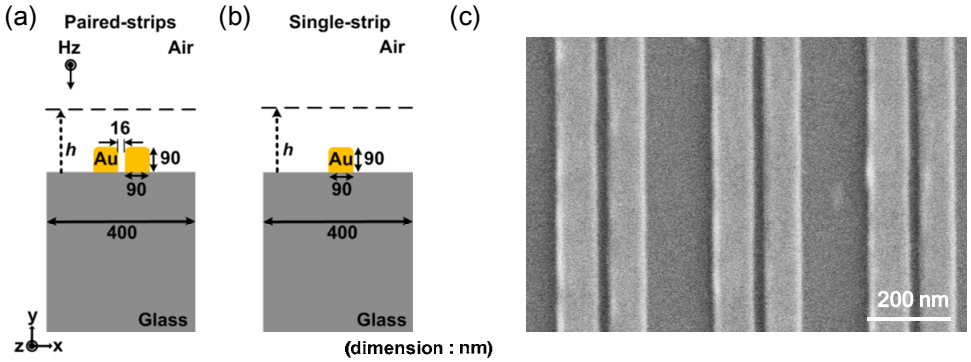

Fig. 1. Different types of nanostructures: Fig. 1(a), paired-strips nanoantennas; Fig. 1(b), single-strip gratings; and Fig. 1(c), scanning electron microscope image of paired-strips nanoantennas.

#205580 - $15.00 USD Received 10 Feb 2014; revised 28 Apr 2014; accepted 8 May 2014; published 19 May 2014

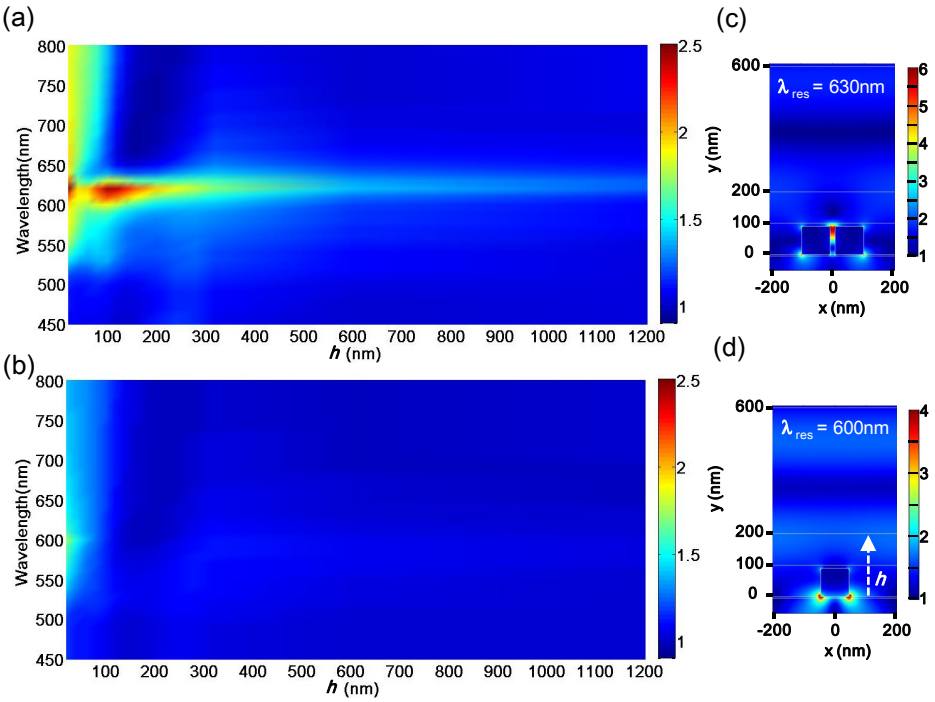

Fig. 2. Normalized average electric field (color scale) versus wavelength (vertical axis), at different integral regions (horizontal axis), for: Fig. 2(a), paired-strips nanoantennas; and Fig. 2(b), single-strip gratings. Figures 2(c) and 2(d) show the 2D distributions of the electric field enhancement ratio at resonant wavelengths (using the no metal structure model as the reference) for: Fig. 2(c), paired-strips nanoantennas; and Fig. 2(d), single-strip gratings. The value E_{ref} is the average electric field without the metallic nanostructure and the normalized average electric field is E_{avg}/E_{ref}.

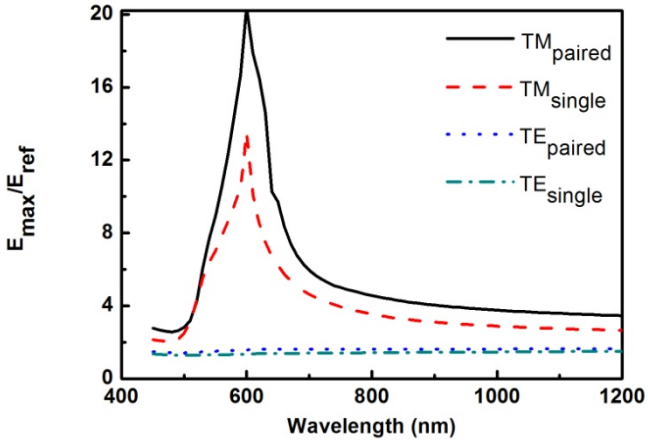

Fig. 3. Normalized maximum electric field versus wavelength for paired-strips and single-strip nanostructures, under TE and TM illumination. The value E_{ref} is the maximum electric field without the metal, for both TE and TM illumination.

3.2 Distinct types of the absorber layer

As discussed previously, the maximum enhancement would occur with a slab thickness, h = 100 nm, therefore, we choose the absorber layer thickness to be 100 nm, so that the

#205580 - $15.00 USD Received 10 Feb 2014; revised 28 Apr 2014; accepted 8 May 2014; published 19 May 2014

refractive index varies as 1 + *i*0.01, 1.33 + *i*0.01, 1.55 + *i*0.01, and 2 + *i*0.01. Figures 4 and 5 show the configuration and simulation results for modifying the real part of the refractive index for the surrounding medium.

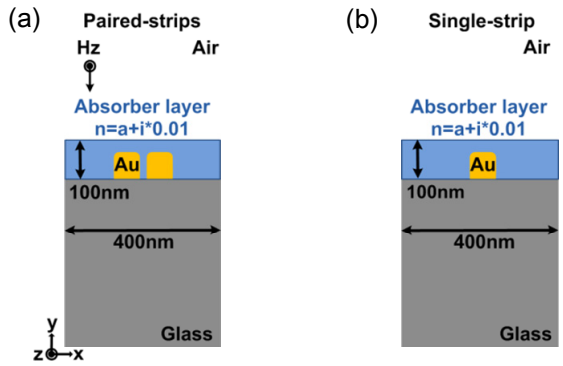

Fig. 4. Two types of nanostructures that are positioned on the bottom of a distinct absorber layer: Fig. 4(a), paired-strips nanoantennas; and Fig. 4(b), single-strip gratings.

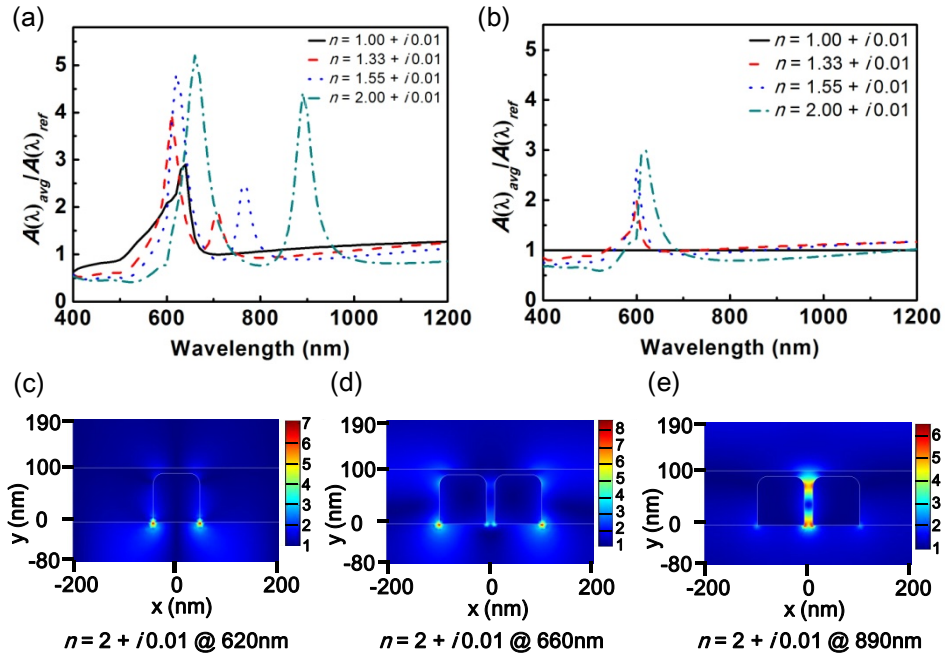

Fig. 5. Normalized average absorption ($A(\lambda)_{avg}$ /$A(\lambda)_{ref}$) versus wavelength for: Fig. 5(a), paired-strips nanoantennas; and Fig. 5(b), single-strip gratings using different refractive index absorber layers (n = a + *i*0.01, where a = 1, 1.33, 1.55, and 2). Figures 5(c)-5(e) show the 2D distributions of the electric field enhancement ratio, at absorption peaks for the n = 2 + *i*0.01 absorber layer. The minimum value of the electric field in Figs. 5(c)-5(e) is used as the reference value. The ratios shown in the figures are: Fig. 5(c), for single-strip gratings; Fig. 5(d), for paired-strips nanoantennas; and Fig. 5(e), for the second peak at longer wavelengths of paired-strips nanoantennas. The value $A(\lambda)_{ref}$, is $A(\lambda)_{avg}$ for a single-strip, using n = 1 + *i*0.01.

In Fig. 5(a), the second peak occurred at longer wavelengths in the absorption spectrum as the electric field was concentrated in the gap, shown in Fig. 5(e). When the refractive index increased, the absorption peak shifted to longer wavelengths, and the corresponding absorption increased. Figures 5(c)-5(e) show that the localized electric field is located around

#205580 - $15.00 USD Received 10 Feb 2014; revised 28 Apr 2014; accepted 8 May 2014; published 19 May 2014

the corner of gold nanostructures. However, the enhancement occurs near the top of the metal, as can be seen in Figs. 5(d)-5(e), only for paired-strips nanoantennas. The peak near a wavelength of 600 nm for paired-strips nanoantennas is more than 1.5 times larger than for the single-strip peak, for all values of the refractive indices for the absorber layers (Re(n) = 1, 1.33, 1.55, and 2). Clearly, the near fields' enhancement in the gaps contributes to the second peak in the absorption spectra for the paired-strips nanoantennas, which produces a more broadband average absorption curve.

3.3 Distinct ultrathin absorber layer

According to Tsai *et al.* [31], a larger attenuation coefficient in the active layer would suppress the plasmon excitation. They discussed the improvement of the absorption enhancement by tuning the imaginary part of absorber layer's dielectric function. Hence, based on the results shown in Figs. 4 and 5, the refractive index of the absorbing thin-film is modified from 1.3 to 4.7, to investigate the relation between the real part of refractive index and the resonance mode.

Plasmonic structures may produce three ways to achieve light trapping in absorber layers [32]. Firstly, metallic nanoparticles can be used as subwavelength scattering elements to couple and trap light into an absorbing thin-film [25, 26, 33, 34]. Secondly, another process for light trapping is by excitation of localized surface plasmons in metallic nanoparticles embedded in the absorber layer. Thirdly, a corrugated metallic film on the back surface of a absorber layer can couple incident light into SPP or photonic modes [28]. Figure 6(a) presents a metallic paired-strips nanoantenna grating sitting at the bottom of the absorber layer, which would take advantage of effective coupling to waveguide modes (Fabry-Perot and SPPs resonance).

In Fig. 6(b), curve #1 represents the enhanced average absorption produced by surface plasmon resonance in the gap, and Fig. 6(c) shows the corresponding electric field distribution in curve #1. Moreover, Figs. 6(d) and 6(e) show the electric field distribution in curve #2 and curve #3. Figure 6(b) shows higher average absorption in curve #3, attributed to the larger electric field distribution. Interestingly, curve #3 only appears when the refractive index is higher (n > 2.5). More resonance modes would appear as the refractive index increases, accompanied by an increased optical path length, which would increase the time the light remains in the absorber layer. Hence, the number of local maxima of absorption would increase (*e.g.* a refractive index of 2 produces two local maxima, while a refractive index of 4 shows four local maxima) and could achieve a higher overall average absorption. It can be inferred that the broader resonance may be related to a higher refractive index.

3.4 Distinct thickness of absorber layer

Engineering the thickness of the absorber layer is very important to optimize effective average absorption. In order to build a simple model for analysis, two absorber layers are chosen such that the refractive indices are $n = 1 + i0.01$ and $n = 2 + i0.01$, to investigate the optimized absorber layer by varying its thickness from 20 to 300 nm.

In Fig. 7, the diffraction mode is at a wavelength ~600 nm, which is determined by the nanostructures' period and the refractive index of the substrate. Figures 8(a) and 8(b) represent the field distributions corresponding to the diffraction mode for both a paired-strips nanoantenna and a single-strip grating. For all thicknesses, from 20 nm to 300 nm, significantly higher average absorption exists near a wavelength of 600 nm, due to the diffraction mode. Furthermore, there is also a cavity resonance mode, shown by the white

#205580 - $15.00 USD Received 10 Feb 2014; revised 28 Apr 2014; accepted 8 May 2014; published 19 May 2014

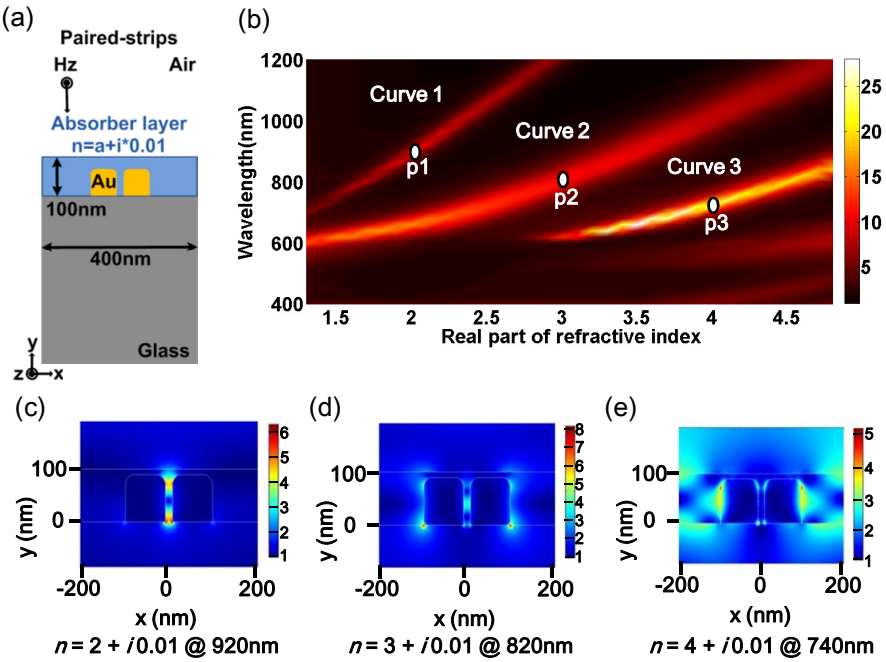

Fig. 6. (a) Paired-strips nanoantennas are positioned at the bottom of an ultrathin absorber layer (thickness = 100 nm). Figure 6(b), the normalized average absorption (color scale) versus wavelength (vertical axis) for a given refractive index (horizontal axis) which ranges from n = 1.3 + *i*0.01 to n = 4.7 + *i*0.01. Figures 6(c)-6(e) show the 2D distributions of the electric field enhancement ratio for each curve in Fig. 6(b). The minimum value of electric field in these three figures is used as the reference. Figure 6(c) shows the distribution for point p1 on curve 1, Fig. 6(d) for point p2 on curve 2, and Fig. 6(e) for point p3 on curve 3. The minimum value of average absorption in Fig. 6(b) is used as a reference for the normalized calculation.

dashed-lines in Figs. 7(b) and 7(d). Cavity resonance modes are determined by the thickness and refractive index of the absorber layer. The cavity resonance mode can be calculated by using Eq. (4),

$$L = \frac{\lambda}{2n} m \tag{4}$$

where L is the length of the cavity, n is the absorber layer's refractive index, and m is an integer.

Table 1 shows the absorption enhancement factor (g) for absorber layers with different thicknesses and Re(n) = 2. For paired-strips nanoantennas, for an absorber layer thickness of 20 nm, g = 30, while for thicknesses of 80 nm and 100 nm, g has values of 10 to 20, respectively. However, for single-strip gratings, the best value, g = 18.5, corresponds to a thickness of 160 nm. Figures 7(a) and 7(b) show the absorption spectra obtained for paired-strips nanoantennas with absorber layers with different refractive indices, $n = 1 + i0.01$ and $n = 2 + i0.01$. An enhancement mode appeared at a wavelength of λ_2 for $n = 2 + i0.01$, and the local maximum absorption had a redshift as the thickness of absorber layer increased from 0 nm to 100 nm. This is consistent with the literature, which states the resonance wavelength would have a redshift when the nanoparticles are embedded in the host [35–37]. As the thickness increases, all the nanoparticles would be covered, and in Fig. 7(b), it's clear the resonance mode located at the wavelength λ_2, would have a significant redshift, until the nanoparticles are completely embedded in the absorber layer.

#205580 - $15.00 USD Received 10 Feb 2014; revised 28 Apr 2014; accepted 8 May 2014; published 19 May 2014

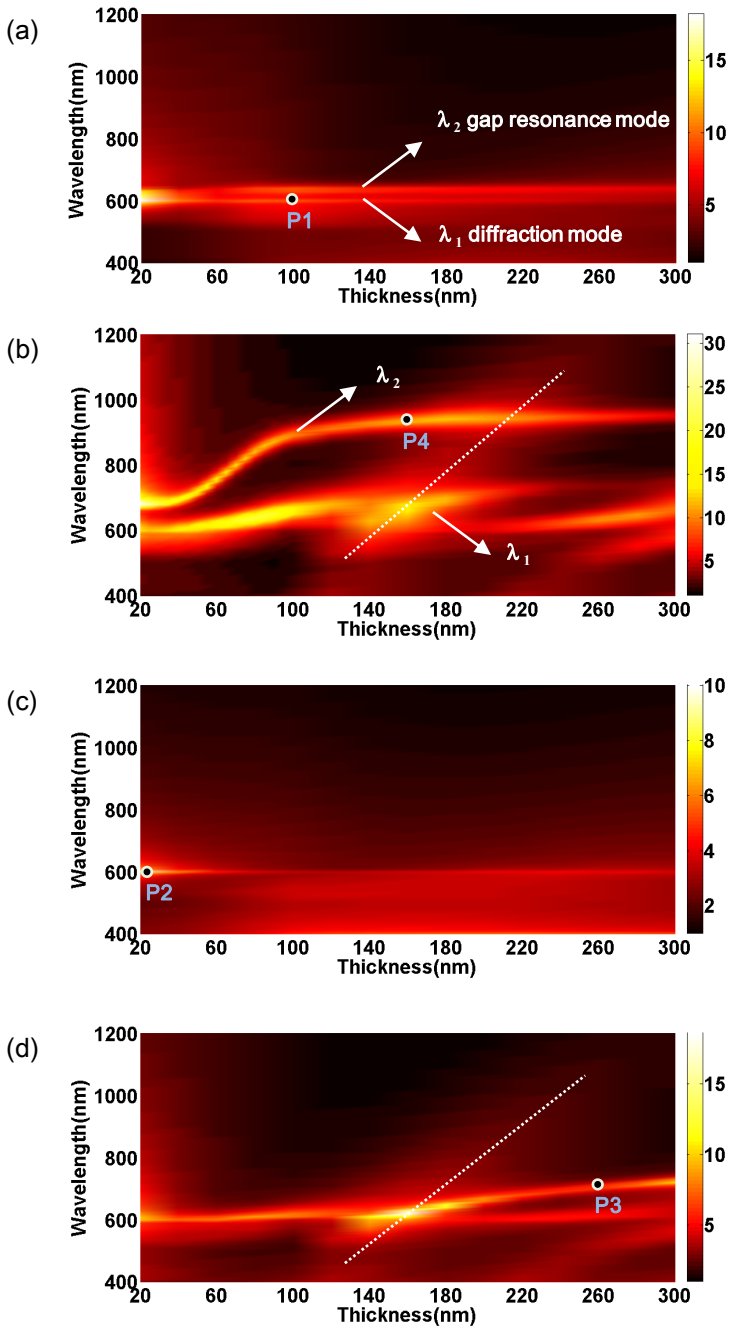

Fig. 7. Normalized average absorption (color scale) versus wavelength (vertical axis) using varying thicknesses of the absorber layer (horizontal axis), which ranges from 20 to 300 nm. Paired-strips and single-strip nanostructures, embedded in absorber layers with two values of refractive index absorber layer (n = 1 + i0.01 and n = 2 + i0.01), are discussed: Fig. 7(a), paired-strips, Re(n) = 1; Fig. 7(b), paired-strips, Re(n) = 2; Fig. 7(c), single-strip, Re(n) = 1; and Fig. 7(d), single-strip, Re(n) = 2. The reference for the normalized calculation is the minimum value of the average absorption in Figs. 7(a)-7(d).

#205580 - $15.00 USD Received 10 Feb 2014; revised 28 Apr 2014; accepted 8 May 2014; published 19 May 2014

Table 1. Absorption enhancement factor of an absorber layer with $n = 2 + i0.01$and different thicknesses

Thickness (nm)	Paired-strips (g, λ_1(nm))	Paired-strips (g, λ_2(nm))	Single-strip (g, λ(nm))
20	(13.1, 600)	(31.0, 680)	(9.6, 600)
80	(20.9, 640)	(12.1, 840)	(8.8, 610)
100	(16.7, 660)	(10.4, 890)	(7.8, 610)
160	(14.0, 670)	(11.0, 930)	(18.5, 620)

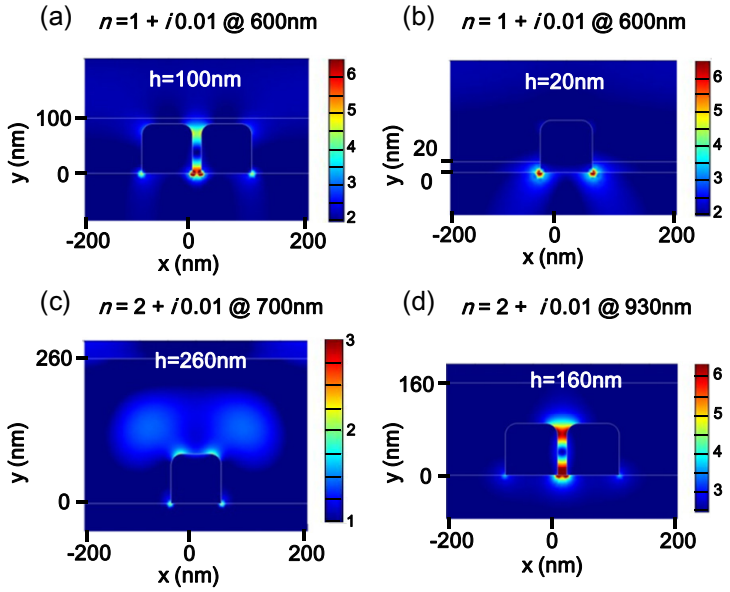

Fig. 8. The 2D distributions of electric field enhancement ratio for four conditions in Fig. 7: Fig. 8(a), for point P1 in Fig. 7(a); Fig. 8(b), for point P2 in Fig. 7(c); Fig. 8(c), for point P3 in Fig. 7(d); and Fig. 8(d), for point P4 in Fig. 7(b). The minimum value of electric field in Figs. 8(a)-8(d) is used as a reference for the electric field enhancement ratio calculation.

Figures 7(c)-7(d) show the absorption spectra of single-strip gratings embedded in different absorber layers, with $n = 1 + i0.01$ and $n = 2 + i0.01$. For $n = 2 + i0.01$, the optimized thickness of the absorbing layer is 160 nm. Increasing the thickness to more than 180 nm, another resonance mode would appear in the plot. Figure 8(c) shows the corresponding electric field distributions for an absorber layer with a thickness of 260 nm. On the other hand, for the case of paired-strips nanoantennas, an additional enhancement occurs because of the interaction within the gap, if the nanoparticles are close enough [15, 17, 38]. In Fig. 8(d), it's clear that the enhanced average absorption is due to the electric field concentrated in the gap for the paired-strips nanoantenna. As shown in Figs. 2(a) and 2(b), the average electric field would be larger in the region near the substrate, or on top of the nanoparticles, for the case in which paired-strips nanoantennas are sitting on the glass substrate in air. Similarly, as shown in Figs. 7(a)-7(d), the localized maximum absorption happens when using an ultrathin thickness of 20 nm or a slightly thicker 100 nm. In Fig. 7, the enhanced absorption is due to three main effects: the diffraction mode, resonance in the gap, and the cavity constructive interference mode. To determine the optimal thickness, the results here show the thinner optimized thickness, 20 nm, would correspond to the gap resonance mode. Moreover, the slightly thicker optimized thickness, 100 nm, would produce both the diffraction mode and the gap resonance mode at two different wavelengths, with the layer thickness around the height of the nanoparticles. Interestingly, much thicker optimized

#205580 - $15.00 USD Received 10 Feb 2014; revised 28 Apr 2014; accepted 8 May 2014; published 19 May 2014

thicknesses, ~160 nm, would be realized due to both the diffraction and cavity modes at wavelengths ~600 nm.

3.5 P3HT:PCBM as absorber layer

For paired-strips nanoantennas, the average absorption is higher than single-strip gratings because of the resonance of two particles with small gaps and, also, the higher enhancement of the diffraction mode, as discussed previously. Therefore, gold paired-strips nanoantennas could be applied in an organic polymer solar cell by using a commercial material called P3HT:PCBM [31, 39–41] as the absorber layer, to investigate the effect of absorption enhancement on energy harvesting.

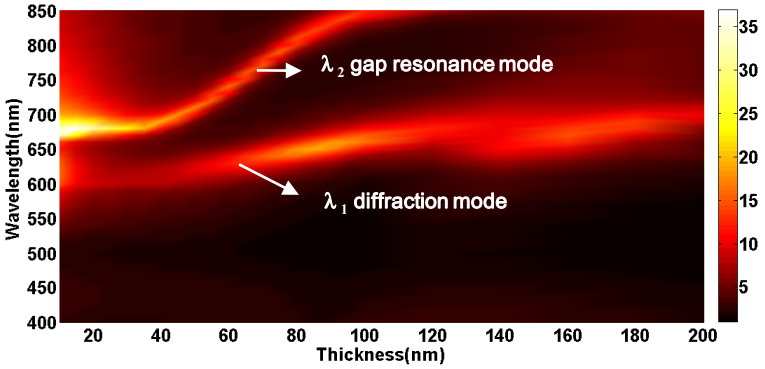

Fig. 9. Normalized average absorption (color scale) versus wavelength (vertical axis) for varying thicknesses of the absorber layer (horizontal axis), which range from 10 to 200 nm, for paired-strips nanoantennas embedded in an absorber layer, consisting of P3HT:PCBM with a 1:1 weight ratio. The minimum value of the average absorption in this 2D map is used as a reference for the normalized calculation.

The optical properties of the active layer using P3HT:PCBM, with a 1:1 weight ratio, are taken from experimental results of the literature [42]. One of this material's advantages is the fabrication process could be carried out simply by spin-coating, which is a low cost manufacturing process. Figure 9 shows the 2D map of the average absorption spectrum using different thicknesses of P3HT:PCBM absorber layers, which range in thickness from 10 nm to 200 nm. The localized maxima of average absorption occurred at an absorber layer thicknesses of 100 nm and 160 nm, and the results correspond to Fig. 7(b). Otherwise, for thicknesses less than 40 nm, the average absorption due to the gap resonance mode is much larger than at a wavelength of λ_1, due to the diffraction mode, and it indicates that the gap resonance mode would dominate the absorption enhancement for these thicknesses. Comparing the result obtained with the absorber layer with $n = 2 + i0.01$, shown in Fig. 7(b), with the absorber layer using P3HT:PCBM, seen in Fig. 9, the enhancement mode shows the same trend. Clearly, our procedure, using a constant value equal to 0.01 for the imaginary part of the refractive index and varying the real part, provides a simple way to investigate the optimal thickness in a specific wavelength range.

4. Discussion

In summary, the average electric field around gold paired-strips nanoantennas may be up to 2.4 times larger than single-strip gratings when they are in air. Also, paired-strips nanoantennas have a 51% higher electric field enhancement than single-strip gratings. In addition, the paired-strips nanoantenna has two peaks in the absorption spectrum, and one is accounted for by the electric field concentrated within the gap. If the real part of refractive index is increased, the plasmonics resonance induced localized field enhancement within the gap might extend beyond near-infrared wavelengths. Moreover, for both paired-strips

#205580 - $15.00 USD Received 10 Feb 2014; revised 28 Apr 2014; accepted 8 May 2014; published 19 May 2014

nanoantennas and single-strip gratings, when the diffraction mode or the gap resonance mode is across the cavity mode, the average absorption could increase by a factor of 10 to 20.

5. Conclusion

This paper compares the absorption enhancement for paired-strips nanoantennas and single-strip gratings. It also discusses the absorption enhancement of paired-strips nanoantennas embedded in ultrathin absorber layers by engineering the thickness and refractive index of the surrounding medium. The optimized thickness of absorber layers is determined by the interaction of three main enhancement effects: diffraction mode, resonance mode in the gap and the cavity mode. The method provided in this work could be further applied to polarization non-sensitive or broadband devices, like nanovoids [43, 44], nanorods [19, 25, 45], mesh [46, 47], and random structure [26, 48], which would be very important in the application of photovoltaic, SERS, and fluorescence enhancement processes, particularly for ultrathin devices.

Acknowledgments

This work is supported by The National Science Council, Taiwan, ROC (Project No. NSC102-2218-E-009-004-MY2). The authors would like to thank Dr. Wei Lee of National Chiao Tung University (NCTU, Taiwan) for his support of providing the computational resource in the Comsol workstation.

#205580 - $15.00 USD Received 10 Feb 2014; revised 28 Apr 2014; accepted 8 May 2014; published 19 May 2014